The spectrum of microdisk lasers

N. C. Frateschi
Instituto de Física–Gleb Wataghin, Universidade Estadual de Campinas, UNICAMP 13083-970, Campinas, São Paulo, Brazil

A. F. J. Levi[a)]
Department of Electrical Engineering, University of Southern California, Los Angeles, California 90089-1111

(Received 6 February 1996; accepted for publication 8 April 1996)

A model for quantitative analysis of microdisk laser emission spectra is presented. Conformal mapping is used to determine radial and azimuthal eigenvalues, eigenvectors, and cavity Q corresponding to leaky optical resonances in an optically transparent dielectric disk. The effects of gain and loss in a microcavity active medium are also included in the model. Our results compare well with experimental data obtained from an InGaAs/InGaAsP quantum well microdisk laser of radius $R=0.8$ μm. © *1996 American Institute of Physics.* [S0021-8979(96)02514-5]

INTRODUCTION

Recently, the possibility of developing semiconductor microlasers using optical resonances of a dielectric disk has been explored. Semiconductor microdisk[1,2] and microcylinder[3] resonant cavities have been studied experimentally with measured lasing emission wavelength at $\lambda=1550$ nm,[4] $\lambda=980$ nm,[3], and $\lambda=620$ nm.[5] Fig. 1(a) shows a scanning electron micrograph of a small, optically pumped microdisk laser. The disk has radius R, thickness L, and is supported by an InP post of rhombohedral cross-section. The multiquantum well active region is surrounded by air with typically 80% optical confinement normal to the plane of the disk. Position in the disk is specified by natural axial coordinate, z, radial coordinate, r, and azimuthal angle, θ. Fig. 1(b) illustrates this coordinate system. With this symmetry optical resonances of an isolated disk are specified by radial quantum number N and azimuthal quantum number M. Figure 2 shows a scanning electron micrograph of a microdisk laser diode, illustrating the more complex geometry of an electrically driven device.

The purpose of this paper is to develop a model for the quasiconfined optical resonances of semiconductor microdisk lasers. First we describe an analytical model for radiative losses and cavity Q for high order M resonances in large disks. We then present the results of using conformal mapping to obtain exact solutions for small optically transparent disks for which low M values are important. The effects of optical gain and loss in the semiconductor medium are then introduced into the model and our results are compared with measured spectra of microdisk lasers.

RESONANCES OF AN IDEAL OPTICALLY TRANSPARENT DIELECTRIC DISK

The design and optimization of a semiconductor microdisk laser is critically dependent on the Q of optical resonances as well as the spectral and spatial overlap of these resonances with the active medium. Microdisk lasers typically consist of a quantum well active region that can exhibit optical gain at, for example, a wavelength $\lambda=1550$ nm. For such devices disk radius is 0.5 μm$<R<10$ μm and thickness is 0.05 μm$<L<0.3$ μm. Because of high optical confinement due to the air–semiconductor interface, it is appropriate to solve the optical field $\psi(r,\theta)$ in the 2-dimensional transverse direction for a medium with effective refractive index $n=n_{\text{eff}}$ in the z direction. We begin our analysis by studying the optical field in an ideal optically transparent dielectric disk.[6] The fact that a semiconductor can also exhibit optical gain and loss at certain optical frequencies will be considered later.

For the case of an optically transparent dielectric we seek solutions to the Helmholtz equation. In this case, the optical field is separable in r and θ so that $\psi(r,\theta)=R(r)e^{z\theta}$ and we may write

$$r^2\frac{d^2}{dr^2}R(r)+r\frac{d}{dr}R(r)+(k^2r^2-Z^2)R(r)=0 \tag{1}$$

and

$$\frac{d^2}{d\theta^2}\Theta(\theta)-Z^2\Theta(\theta)=0, \tag{2}$$

where $k=n_{\text{eff}}\omega/c$ and Z is, in general, a complex constant. Two polarizations may be studied for the TE (TM) resonance of the slab waveguide. This resonance undergoes a TM (TE) reflection at the disk's edge with the magnetic (electric) field in the $\hat{\mathbf{z}}$ direction $H_z(r,\theta)(E_z(r,\theta))$ with $n_{\text{eff}}=n_{\text{eff}}^{\text{TE(TM)}}$.

One simplifying approach assumes that optical resonances may be approximated by ''whispering gallery modes'' (WGMs). WGMs are obtained via application of the boundary condition $\psi_{\text{in}}(R,\Theta)=0$, where ψ_{in} is the optical field for $r\leqslant R$. In this situation

$$\psi_{\text{in}}(r,\theta)=A_{M,N}J_M(rn_{\text{eff}}\omega_{M,N}/c)e^{iM\theta}, \tag{3}$$

where J_M are Bessel functions of integer order $Z\equiv M=0,\pm1,\pm2,\pm3,...$ and $A_{M,N}$ is a normalization constant. The boundary condition results in resonance frequencies $\omega_{M,N}=x_M^N c/n_{\text{eff}}R$ where x_M^N is the Nth zero of $J_M(r)$ and $N=1$ for WGMs. One may show that the instantaneous Poynting vector for $N=1$ is of the form

a)Electronic mail: alevi@usc.edu

 0021-8979/96/80(2)/644/10/$10.00

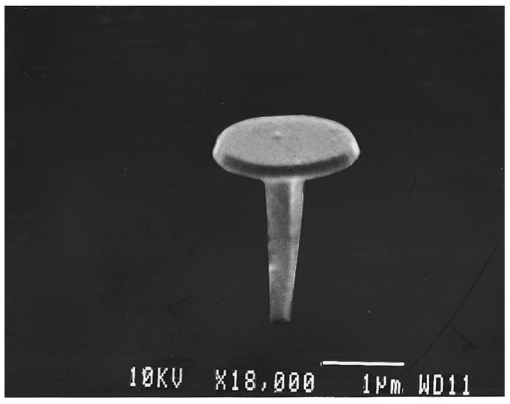

(a)

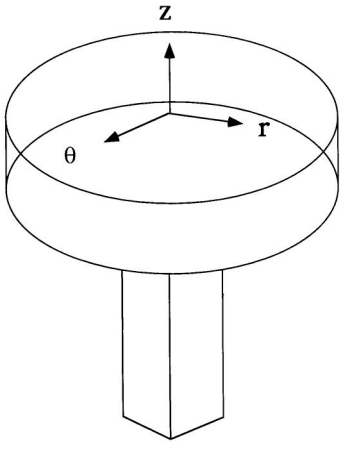

(b)

FIG. 1. (a) Scanning electron micrograph of a small, optically pumped microdisk laser. A 1 μm scale is indicated. (b) Coordinate system utilized in the microdisk calculation.

$$\mathbf{k}_M = k_\theta(r) M \cos^2(M\theta - \omega t)\hat{\boldsymbol{\theta}} + k_r(r)\sin(2M\theta - \omega t)\hat{\mathbf{r}}. \tag{4}$$

This describes optical-ray propagation in the $\hat{\boldsymbol{\theta}}$ direction (clockwise or counterclockwise depending on the sign of M) with $2M$ symmetrical mirror reflections with respect to the radial direction. For such a solution, the time average energy flux is given by $\mathbf{S} \propto M\hat{\boldsymbol{\theta}}$ and, consequently, no optical energy escapes the disk in the radial direction.

A physically more reasonable solution is obtained by allowing complex eigenvalues, $Z = M + i\alpha R$, as solutions to the Helmholtz equation. This results in ψ having exponential decay for the component $\psi_\theta(\Delta\theta) = e^{-2\mathcal{I}(Z)\Delta\theta}$ with $\Delta\theta$ propagation in the azimuthal direction and Bessel-type functions of ''complex order'' result in finite radial transmission. For large disks we consider the limit of high-order M and $N=1$. In this limit α approaches zero and a WGM model is a good approximation. For small disks, M is small since the resonance wavelengths can not be smaller than the active region emission wavelength in the material $(x_M^N \leqslant 2\pi R n_{\text{eff}}/\lambda)$. In this situation α is finite, there is a significant radial flux of energy, and physically meaningful solutions for ψ depart considerably from the WGM picture.

For high-order M and $N=1$ the WGM model is a good approximation and we assume resonant modes of a microdisk impinge at the disk's edge with an off-plane angle η given by the confinement perpendicular to the disk's plane and a glancing angle $\xi(M)$. The off-plane angle is assumed to be very small due to the high confinement of the optical mode in the disk's plane. However, we note that after leaving the disk's edge one might expect that the lack of confinement should result in off-plane emission with a diffraction angle $\eta_{\text{dif}} \approx \lambda/L$. According to the above discussion, WGMs follow a polygonal optical path of length L_T with $2M$ sides. Therefore, the glancing angle $\xi(M)$ and corresponding total optical path length are related to a WGM of order M by $\xi(M) = (M-1)\pi/2M$ and $L_T(M) = (2M)2R\sin(\pi/2M)$, respectively. Higher-order modes have greater incidence angle approaching $\xi = 90°$ and $L_T = 2\pi R$ as M approaches infinity. Snyder and Love[7] showed that for wavelengths much smaller than the radius of curvature optical transmission, $T(\xi)$, at a curved interface is related to the polarization dependent Fresnel coefficient for planar interfaces, $T_F(\xi)$, via $T(\xi) = |T_F(\xi)|C(\xi)$, where $C(\xi)$ is a polarization independent curvature coefficient. For large M, or equivalently incidence angle wider than the critical angle $\xi(M) \gg \xi_c$, $T_F(\xi) = 1$ for both polarizations. The Appendix shows that for a WGM resonance the optical transmission approaches $T_M = \exp[-(2\pi R\eta_{\text{eff}}/\lambda)(2/3)\cos^3_{\xi_c}]$. Using the WGM boundary conditions we obtain $T_M = \exp[-(x_{M,1})(2/3)\cos^3_{\xi_c}]$ and, therefore, transmission becomes only weakly dependent on the effective index through $\xi_c = \arcsin(1/n_{\text{eff}})$ and essentially independent of disk radius. Since $x_{M,1}$ increases monotonically with M, the transmission is smaller for higher order resonances. The energy associated with a resonance M is $U_M(t) = U_0 e^{i(2M\theta - 2\omega t)}$. Given an azimuthal phase velocity $v = \omega/M$ the time, Δt, for a bounce occurring in $\Delta\theta = 2\pi/2M$ is $\Delta t = \Delta\theta/v = \pi/\omega$. Hence, the typical optical feedback time $\Delta t \sim 2.5$ fs is very short. The energy reduction with time for a lossless dielectric medium is then $\Delta U_M(t)/\Delta t = -[U_M(t)T_M](\omega/\pi)$. For large M, $\Delta\theta/\Delta t$ approaches $\partial\theta/\partial t$ and the cavity Q defined by $U_M(t) = U_0 e^{(-\omega t/Q)}$ is given by $Q_M = \pi/T_M$ or

$$Q_M = \pi e^{((2/3)x_{M,i}\cos^3\xi_c)}. \tag{5}$$

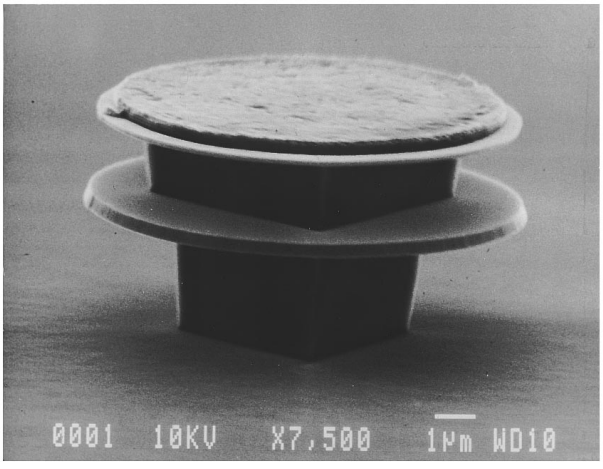

FIG. 2. Scanning electron micrograph of a electrically pumped microdisk laser diode. The device has a radius about 5 μm and electrical current is injected from the top metal contact.

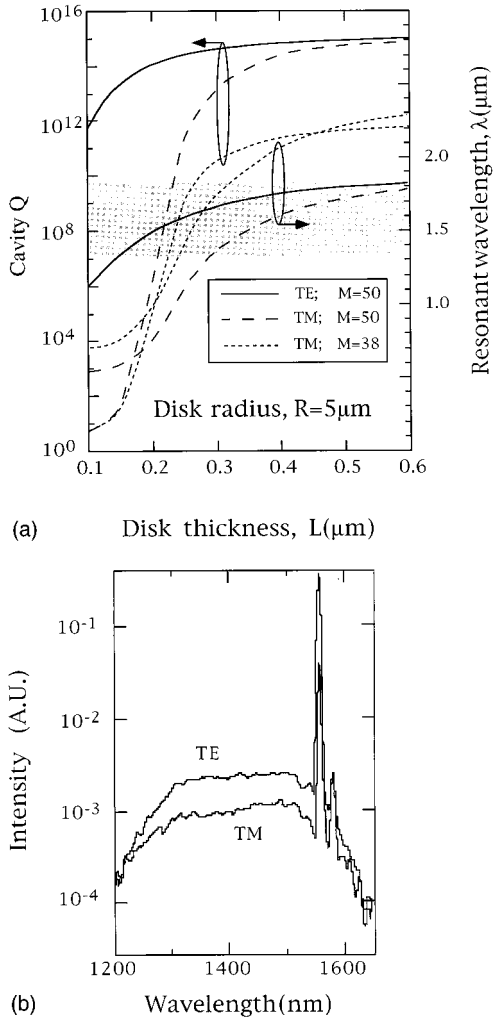

FIG. 3. (a) Calculated cavity Q and resonance wavelength for TE and TM modes with $M=50$ and $M=38$ plotted as a function of disk thickness, L. (b) Measured polarization resolved spectra for a microdisk laser diode with $In_{0.53}Ga_{0.47}As$ active region, $L=0.29$ μm and $R=5$ μm. Spectrometer resolution is 5 nm and room temperature injection current is 8 mA. Threshold current is 2 mA.

We should remark that for these large disks the cavity Q depends explicitly on polarization, disk geometry, and material through ξ_c. The critical angle ξ_c is a function of n_{eff} that depends on polarization, disk thickness L, and material index of refraction. The dependence on disk radius is implicit since Eq. (5) is only valid for $R \gg \lambda/n_{\text{eff}}$ and also M is limited by $x_M^N \leqslant 2\pi R n_{\text{eff}}/\lambda$ as λ is constrained to values within the spontaneous emission line width. Figure 3(a) shows cavity Q calculated as a function of disk thickness, L for a large disk with $R=5$ μm. The material refractive index is $n=3.5$ and no dispersion was considered. Results for modes TE with $M=50$ and TM with $M=50$ and $M=38$ along with the corresponding calculated resonance wavelengths are plotted in Fig. 3(a). The shaded area in the plot represents a typical $In_{0.53}Ga_{0.47}As$ active region emission wavelength. Thinner disks have smaller n_{eff} and, consequently, larger critical angle resulting in lower Q for a given resonance M. For any mode, TE polarization has higher Q than TM polarization. This is accentuated for $L<L_0$ where L_0 is a critical disk thickness below which a great reduction in $n_{\text{eff}}^{\text{TM}}$ occurs. However, for high-order resonances and $L \geqslant L_0$, Q is so high for both polarizations that polarization independent processes mask any polarization selectivity of the cavity. Figure 3(b) shows results from experiments which measure polarization of light emitted from microdisk laser diodes with an $In_{0.53}Ga_{0.47}As$ active region, $L=0.29$ μm and $R=5$ μm. From Fig. 3(a) $L=0.29$ μm and $R=5$ μm, modes TE, $M=50$ and TM, $M=38$ have resonance wavelengths that best overlap with the active region emission. As expected these modes result in a peak in the spectra for both polarizations near $\lambda=1.56$ μm (dispersion must be considered for an exact peak position calculation). The fact that the TE mode has twice the intensity of the TM mode is believed to originate from the polarization dependence of the active region emission.[8]

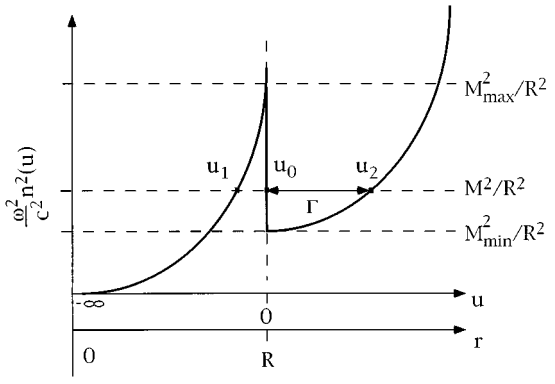

FIG. 4. Index of refraction profile for the slab waveguide in the transformed space (u,v). The reflection points (u_0,u_1,u_2) are shown for a resonance with $M_{\text{Min}} \leqslant M \leqslant M_{\text{Max}}$.

CONFORMAL MAPPING

As mentioned previously, for small disks with higher losses and/or resonant wavelengths comparable to the disk radius the WGM approach to modeling is inappropriate. As a first step to a better model for microdisks we adapt a technique used by Heiblum and Harris to calculate loss in curved optical waveguides.[9] In their work, a conformal transformation $u+iv=f(r,\theta)=R\ln[re^{i\theta/R}]$ is applied to the two-dimensioned Helmholtz equation. Recently, Chin *et al.* also applied this technique to calculate resonance wavelengths in microdisk lasers. Unfortunately, Chin *et al.*[10] assumed that the eigenvalue solutions to the Helmholtz equation are real. This is just the WGM approximation, which, as discussed previously, is not valid for the small disks of interest. In our present work we are mainly concerned with calculating the cavity losses and spectral position for optical resonances in small microdisk lasers. Using conformal mapping, the problem is transformed into an asymmetric slab waveguide in the $\hat{\mathbf{v}}$ direction with a varying index of refraction profile $n(u)=n_{\text{eff}}e^{u/R}$ for $r \leqslant R$ and $n(u)=e^{u/R}$ for $r>R$ as illustrated in Fig. 4. Resonances propagate according to $f(u,v)=U(u)e^{i(\beta+i\alpha)}$. For the microdisk resonator $Z=M+i\alpha R$ gives $\psi(r,\theta)=F(r)e^{iM\theta}e^{-\alpha\theta}$ in real space and $\Omega(u,v)=H(u)e^{iM/R\theta}e^{-\alpha\theta/R}$ in the transformed space. That is, a wave propagating in the $\hat{\mathbf{v}}$ direction with a known

propagation constant $k_v = M/R$ with M integer to guarantee a stationary solution in the $\hat{\boldsymbol{\theta}}$ direction and a propagation loss α. A stationary solution is one in which the nodes of $\psi(r,\theta)$ are a constant in time. In the $\hat{\mathbf{u}}$ direction

$$\frac{d^2H(u)}{du^2} + \frac{\omega^2}{c^2}\,\overline{n^2}(u)H(u) = 0, \tag{6}$$

where plane waves in each infinitesimal slice δu propagate in the $\pm\hat{\mathbf{u}}$ direction through an index of refraction

$$\overline{\eta}(u) = \sqrt{n^2(u) - \left(\frac{c}{\omega}\,(M/R + i\alpha)\right)^2}\,. \tag{7}$$

These waves change phase by $\delta\phi = (\omega/c)\,\overline{\eta}(u)\,\delta u$ with propagation in the continuous medium and are reflected at the discontinuities of $\overline{\eta}(u)$. For $\alpha \ll M/R$ reflections occur at the roots of $n(u) = (c/\omega)M/R$, $u_1 = R\,\ln[(c/\omega)M/Rn_{\text{eff}}]$ for $u<0$ and $u_2 = R\,\ln[(c/\omega)M/R]$ for $u>0$ and at the physical interface at $u_0 = 0$. Figure 4 shows these reflection points for a given M. Note that u_1 and u_2 are metal-type reflections while u_0 is a dielectric-type reflection. A stationary solution in u will require a round trip phase change $N2\pi$, $N = 1,2,3,...$, between u_1 and u_0. For u_1 to exist $M < M_{\max} = 2\pi R n_{\text{eff}}/\lambda$ must be satisfied and, hence, the maximum allowed M is limited since λ is restricted to the active region emission linewidth. At u_0 the phase change depends on phase response from the combined dielectric- and metal-type reflections that occur at u_0, the segment Γ, and u_2. Also, it depends on the polarization since, for the TM (TE) slab resonances, TE (TM) reflections at the edge, $\nabla_u H(u)[\nabla_u H(u)/\epsilon]$ is continuous. If these reflections are in phase, then high reflectivity results and a quasiconfined stationary resonance exists. The contribution from the virtual reflection point u_2 is essential for this calculation. Ignoring u_2 and with k_ν complex any frequency ω may be associated with a stationary state as long as a finite loss is assumed. In other words, neglecting u_2 leads to a monotonic functional dependence between frequency and loss (consequently a broad spectrum $\omega_{M,N}(\alpha)$ for each resonance). However, the requirement on round-trip phase and constructive reflection at the $u_0 - \Gamma - u_2$ mirror combination result in two equations involving α and ω for a given M and N. A quasiconfined stationary resonance M with round-trip phase $N2\pi$ has a center frequency $\omega_{M,N}$ and loss $\alpha_{M,N}$. The energy in a given quasiconfined state is given by

$$U = U_0 e^{-2\alpha_{M,N}R\theta} e^{i(2M\theta - 2\omega_{M,N}t)}, \tag{8}$$

with a time decay given by

$$U = U_0 e^{-(2\omega_{M,N}\alpha_{M,N}R/M)t}. \tag{9}$$

Therefore $Q_{M,N} = M/2\alpha_{M,N}R$. We note that when u_2 does not exist ($M < M_{\min} = 2\pi R/\lambda$) broad stationary (but not quasiconfined) states are allowed since photons leaving the disk only experience a relatively low reflectivity dielectric interface in a situation physically analogous to below critical angle ξ_c incidence. We expect, therefore, sharp spectral lines with high cavity Q to occur within the broad range of non-quasiconfined spontaneous emission.

Figure 5 shows measured spectra for a microdisk with $R = 0.8$ μm and $L = 0.18$ μm. We assume the medium has an

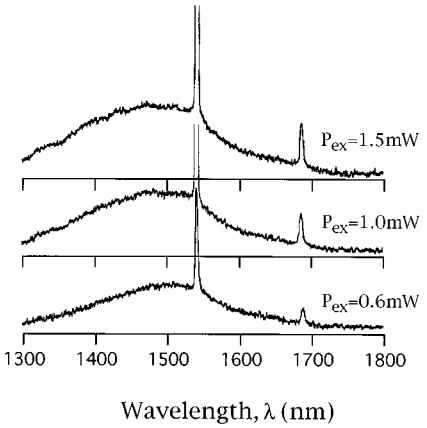

FIG. 5. Room temperature photoluminescence spectra of $R = 0.8$ μm radius microdisk laser. Light is collected from the top of the disk with a 0.5 numerical aperture lens. P_{ex} is the total incident excitation power with $\lambda = 0.85$ μm (Ref. 4).

average refractive index $n = 3.456 + 0.333(\hbar\omega - 0.74\ \text{eV})$.[4] Emission peaks at $\lambda_{5,1} = 1542$ nm and $\lambda_{4,1} = 1690$ nm are observed in a spontaneous emission background ranging from $\lambda = 1300$ nm to $\lambda = 1800$ nm. To obtain the spectra for this structure we fit the calculated effective index dispersion $n_{\text{eff}} = n_{\text{eff}}^{\text{TE}} = 1.494 + 1.427\ \hbar\omega$. We have neglected TM emission since $n_{\text{eff}}^{\text{TM}}$ is too small to allow resonances within the spontaneous emission range. For this n_{eff} and the wavelength range of interest, we find for quasiconfined optical resonances that M is limited to $3 < M < 13$. Figure 6 shows the calculated spectral lines for this disk where resonances with $Q > 0.2$ were considered. The cavity Q increases exponentially with M and we observe that it reduces rapidly with increasing N. The resonances (5,1) and (4,1) match very well

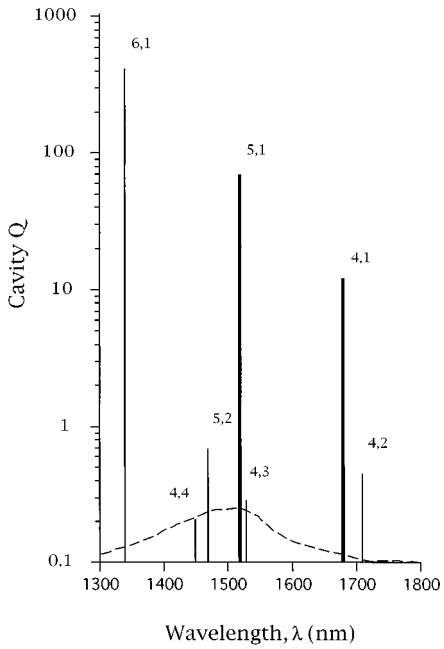

FIG. 6. Calculated spectral lines with respective cavity Q for resonances in the $R = 0.8$ μm radius microdisk laser of Fig. 5. The broken line represents the experimentally observed spontaneous emission.

the measured resonances shown in Fig. 5 where a combination of higher Q and greater overlap with the spontaneous emission lead to the dominating resonance at $\lambda_{5,1}=1540$ nm. The highest Q resonance in this range (6,1) is not seen in the spectra because, in contrast to our optically transparent dielectric disk model, the semiconductor disk is strongly absorbing at this wavelength. $M=7,8,9$ with higher Q are not depicted because for these resonances $\lambda<1300$ nm. We consider remarkable that the above model, which describes resonances in an optically transparent medium agrees so well with the experimental results. Even better agreement is possible by including effects due to the presence of the active semiconductor medium. For example, suppression of resonance (6,1) will naturally evolve from such an approach.

MODEL FOR GAIN AND LOSS

Any model of microdisk lasers must include the effects of semiconductor optical gain and loss. Because electron scattering rates, band gap renormalization, gain bandwidth, and inverse photon lifetime can all have a similar energy scale, it is necessary to consider the impact of each process on laser performance. An ultimate objective is the development of a self-consistent theory that describes the complete interacting photon–electron system. While significant progress has been made in this direction,[11] at present we chose an approach that is unencumbered by such additional complexity.

We start by considering electrons in thermal equilibrium at temperature T and distributed according to the Fermi functions $f_c(k)$ and $f_v(k)$ for the conduction and valence bands, respectively. Following Chuang *et al.*,[12] the spontaneous emission rate, or the number of emitted photons per second per unit volume per unity energy interval, is given by

$$R_{\rm sp}(\omega)=N(\hbar\omega)\,\frac{c}{n_g}\,g_{\rm sp}(\omega), \tag{10}$$

at a photon energy $\hbar\omega$, where $N(\hbar\omega)$ is the electromagnetic modal density, $g_{\rm sp}(\omega)$ is conveniently defined to have the same dimensions. (1/cm) as gain and c/n_g is the group velocity for light in the material. For a bulk semiconductor spontaneous emission may be written

$$g_{\rm sp}(\omega)=\frac{\omega}{n_g c\epsilon_0}\,\frac{e^2\hbar^2}{3m_0}\,E_p \times\int_0^\infty \frac{k^2dk}{2\pi^2}\,\frac{1}{E_{cv}^2(k)}\,\frac{\gamma_k f_c(1-f_v)}{[E_{cv}(k)-\hbar\omega]^2+\gamma_k^2}, \tag{11}$$

where γ_k is the electron scattering induced linewidth, $E_{cv}(k)$ is the energy separation between a conduction band electron and a valence band hole assuming k-selection rules, $E_p=2m_0P^2/\hbar^2$, and P is Kane's parameter.[13] We now calculate optical gain $g_{\rm opt}(\omega)$ from the spontaneous emission spectrum using the expression[14]

$$g_{\rm opt}(\omega)=(e^{\beta(\hbar\omega-\Delta\mu)}-1)g_{\rm sp}(\omega), \tag{12}$$

where $\Delta\mu=E_g+\mu_n-\mu_p$ is the separation between electron and hole chemical potential, μ_n and μ_p, respectively, and $\beta=1/k_BT$ where k_B is Boltzmann's constant. Carrier induced band-gap shrinkage is included via $E_g=E_g^0-\zeta n^{1/3}$ where $\zeta=2.2\times10^{-5}$ meV cm and $E_g^0=0.75$ eV is the unrenormalized room temperature band gap for $In_{0.53}Ga_{0.47}As$.[15] Clearly our gain model preserves the simplicity of the density-matrix formulation and satisfies the important thermodynamic requirement that the optical transparency energy occurs at the difference of electron and hole chemical potential, $\Delta\mu$.

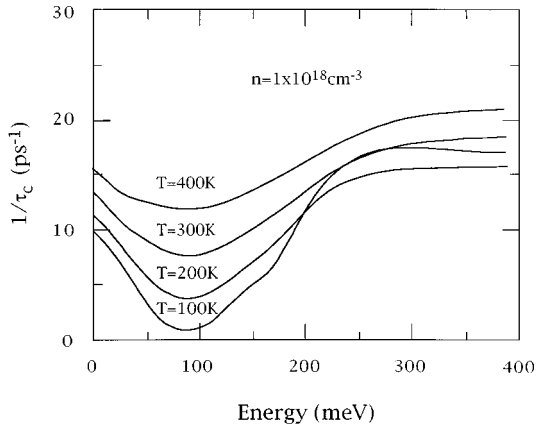

FIG. 7. Calculated reciprocal intraband relaxation time $1/\tau_c$ for bulk $In_{0.53}Ga_{0.47}As$ with conduction band carrier density $n=1\times10^{18}$ cm^{-3} for the indicated temperatures.

The variation in electron scattering with temperature and carrier density may be illustrated by considering the inelastic scattering rate, $1/\tau_c(E)=2\gamma_k/\hbar$, for a central Γ-valley conduction band electron of initial kinetic energy E and wave vector $\mathbf{k}$. Electrons may scatter inelastically, changing kinetic energy by $\hbar\omega$ and changing momentum by $\mathbf{q}$. Scattering rates may be calculated within the random phase approximation using a method (see, e.g., Ref. 16) that relates the electron self-energy to the dielectric response of the semiconductor. Within this formalism, the dielectric response function for a conduction band electron is

$$\epsilon(\mathbf{q},\omega)=\epsilon_\infty\left(1-\frac{\omega_{\rm LO}^2-\omega_{\rm TO}^2}{\omega(\omega+i\gamma)-\omega_{\rm TO}^2}\right)+\chi_n(\mathbf{q},\omega), \tag{13}$$

where ϵ_∞ is the high frequency dielectric constant, $\omega_{\rm LO}$ is the longitudinal optic phonon frequency, $\omega_{\rm TO}$ is the transverse optic phonon frequency, γ is a collision broadening term, and $\chi_n(\mathbf{q},\omega)$ is the contribution from n conduction band electrons. In this case the inelastic scattering rate, $1/\tau_n$, is calculated using

$$\frac{1}{\tau_c}=\sum\ \frac{-8\pi e^2}{\hbar^2q^2}\,{\rm Im}\left[\frac{1}{\epsilon(q,\omega)}\right][f(E-\hbar\omega)+g(\hbar\omega)], \tag{14}$$

where the Fermi function $f(E)=1/(e^{(E-\mu_n)/k_BT}+1)$ and the Bose function $g(E)=1/(e^{E/k_BT}-1)$. Figure 7 shows $1/\tau_c$ for bulk $In_{0.53}Ga_{0.47}As$ with a carrier density $n=1\times10^{18}$ cm^{-3} for the indicated temperatures. At room temperature ($T=300$ K) and in the energy range of interest ($E\sim50$ meV) we find the scattering rate is relatively energy insensitive with $1/\tau_c\sim10$ ps^{-1}. To illustrate the temperature sensitivity of $1/\tau_c$, Fig. 8 shows $1/\tau_c$ for $E=50$ meV and $E=150$ meV as a function of temperature for the indicated values of carrier

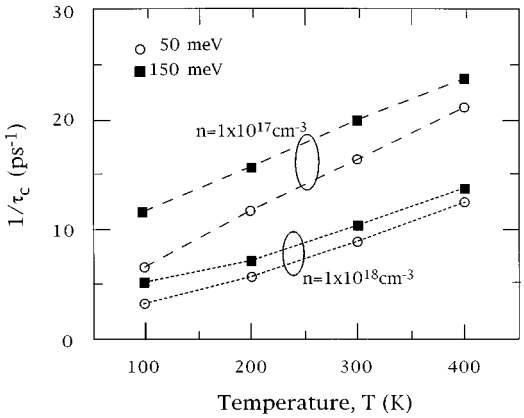

FIG. 8. Calculated reciprocal intraband relaxation time $1/\tau_c$ in $In_{0.53}Ga_{0.47}As$ for $E=50$ meV and $E=150$ meV as a function of temperature for the indicated values of conduction band carrier density n.

density n. For $n=10^{18}$ cm^{-3} the overall scattering rate and its temperature dependence is weak due to electron screening and the fact that the Fermi energy $E_F(T=0\ \mathrm{K}) \geqslant k_B T$ at the temperature range of interest.

The preceding refers to electrons interacting with longitudinal optical phonons and other electrons in the conduction band. However, there is also a temperature dependent contribution to $1/\tau_c$ from conduction band electrons scattering off holes in the valence band that adds a term $\chi_v(\mathbf{q},\omega)$ to $\epsilon(\mathbf{q},\omega)$.[17] For $T=300$ K and $E\sim 50$ meV, this gives a similar contribution so that the total scattering rate for conduction band electrons is $1/\tau_c^{\mathrm{total}} \sim 20$ ps^{-1}. In addition, there is a contribution to the total line broadening due to the self-energy of holes in the valence band. Associated with this self-energy is a lifetime τ_v^{total} so that $2\gamma_k = \hbar(1/\tau_c^{\mathrm{total}} + 1/\tau_v^{\mathrm{total}})$. Because the devices of interest operate with $n \cong p \cong 10^{18}-10^{19}$ cm^{-3} at temperature $T=300$ K, we may approximate $1/\gamma_k$ by a constant electron scattering induced broadening factor with $1/\gamma_k \sim 60$ meV at room temperature. In Fig. 9 we show the calculated optical gain spectrum for $n=1\times10^{17}$ cm^{-3} to $n=1\times10^{19}$ cm^{-3} and using $1/\gamma_k \sim 60$ meV.

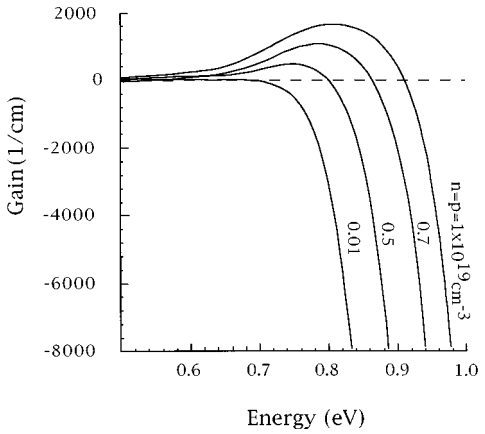

FIG. 9. Calculated room temperature ($T=300$ K) optical gain spectrum in $In_{0.53}Ga_{0.47}As$ for $n=1\times10^{17}$ cm^{-3} to $n=1\times10^{19}$ cm^{-3} with total collision broadening term $1/\gamma_k \sim 60$ meV.

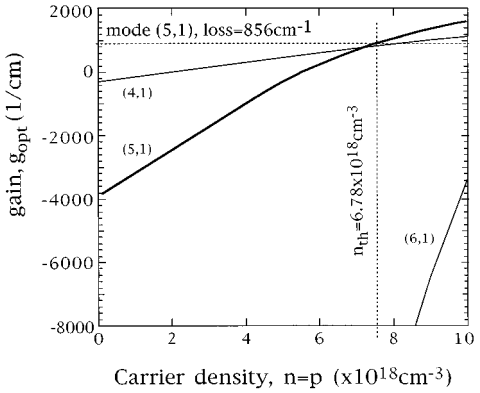

FIG. 10. Calculated g_{opt} vs injected carrier density at the wavelengths corresponding to resonances (4,1), (5,1), and (6,1).

COMPARISON OF EXPERIMENT AND CALCULATION

We introduce gain into our model of the microdisk by assuming a change in optical intensity

$$\Delta I(t) = g_{\mathrm{opt}}(\omega)\Gamma_{M,N} R \Delta\theta(t), \tag{15}$$

to occur in the circular motion of a resonance. Here

$$\Gamma_{M,N} = (1/R)\int_0^R rF^2(r)dr \Big/ \int_0^R F^2(r)dr \tag{16}$$

represents a radial average for the energy maxima position of a given resonance, where $F(r)$ is the radial part of $\psi(r,\theta)$. This approach is a good approximation for resonances $N=1$ with a narrow single intensity maxima near radial position $\Gamma_{M,1}R$ close to the disk's edge. The energy decay in the cavity is now corrected by

$$I(t) = I(t_0)e^{-[2(\omega_{M,R}R/M)(\alpha_{M,N} - g_{\mathrm{opt}}(\omega)\Gamma_{M,N})t]}, \tag{17}$$

where the new quality factor is given by

$$Q = (M/2\alpha_{M,N}R)/[1 - g_{\mathrm{opt}}(\omega_{M,N})\Gamma_{M,I}/\alpha_{M,N}R]. \tag{18}$$

Figure 10 shows the calculated g_{opt} at the wavelengths corresponding to resonances (4,1), (5,1), and (6,1). Analysis of optical resonances based on fixed wavelength gain curves assumes that no change in resonance wavelength occurs due to changes in refractive index with carrier injection. To verify this approximation we have estimated the change in index of refraction from the calculated gain spectrum according to Henry *et al.*[18] Figure 11 shows the calculated change in index of refraction for $n=5\times10^{18}$ cm^{-3} and $n=8\times10^{18}$ cm^{-3}. After including these changes in refractive index we have recalculated the resonances in the disk and found no significant change (less than 1%). This agrees with the observed absence of changes in resonance position when these lasers are pumped under a wide range of carrier concentrations as shown in Fig. 5. Moreover, it explains the good agreement between calculated spectral position for the transparent disk and experimental results.

In Fig. 10, following lasing resonance (5,1), we observe that at $n_{\mathrm{th}}=p_{\mathrm{th}}=6.78\times10^{18}$ cm^{-3} and the threshold gain of $g_{\mathrm{th}}=856$ cm^{-1} equals the losses in the cavity. The threshold gain for the small disk ($R=0.8$ μm) is obtained from $\alpha_{M,N}$

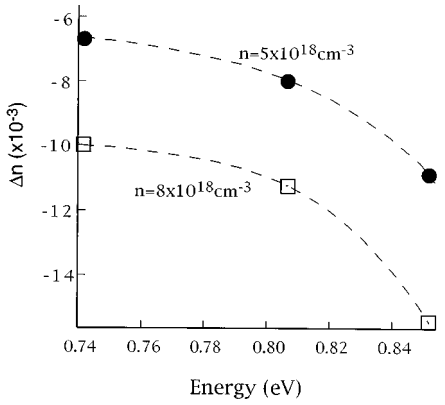

FIG. 11. Calculated values for the index of refraction for $n=5\times10^{18}$ cm^{-3} and $n=8\times10^{18}$ cm^{-3}.

and the optical confinement factor for the structure. It is interesting to consider the behavior of the other two resonances at this carrier density. Associated with resonances (6,1) and (4,1) is $g_{\text{opt}}=-15\,000$ cm^{-1} and $g_{\text{opt}}=800$ cm^{-1}, respectively. Resonance (6,1) has photon energy $E>\Delta\mu$ and negative gain, i.e., absorption, causing a dramatic reduction in Q from $Q_{6,1}=400$ to $Q_{6,1}=3$. On the other hand, resonance (4,1), has positive gain since it occurs on the long wavelength side of the lasing emission. The effect of this is to increase Q from $Q_{4,1}=12$ to $Q_{4,1}=20$. Overall, we expect resonance (6,1) to be very lossy with an approximately 440-nm-wide spectral line and resonance (4,1) with it's higher finesse will have a narrower linewidth of about 84 nm. Qualitatively this explains the suppression of resonance (6,1) and the presence of the narrow peak for resonance (4,1).

To calculate the spectrum and the emission power dependence on pump level, we have to solve the dynamic equations describing device operation. A prerequisite is evaluating the total spontaneous emission rate ($R_{\text{sp}}^{\text{total}}$) and the spontaneous emission coupling coefficient (γ) to resonances. To avoid confusion we define a mode as the exact solution of the lossless eigenvalue–eigenvector problem and a resonance as the finite linewidth standing wave of a practical lossy structure. As a starting point we calculate the total radiative recombination rate for a given carrier density n using

$$R_{\text{sp}}^{\text{total}}=V\int_{-\infty}^{\infty}(c/n_g)N_{\text{BB}}(E)g_{\text{sp}}(E)dE, \tag{19}$$

where $N_{\text{BB}}(E)$ is the black-body radiation interacting with the laser medium. The use of the black-body radiation density of states is only valid if most of the spontaneous emission couples into very lossy resonances or free-modes. We obtain a value $R_{\text{sp}}^{\text{total}}(n)\approx9\times10^{-12}$ n^2(cm^{-3}s^{-1}). No other recombination processes or leakage factors were included in this calculation so that the value of $R_{\text{sp}}^{\text{total}}$ represents a lower bound.

Figure 12(a) shows the measured P_{out} vs P_{ex} plot for the microdisk. This curve can be fit by using the above value for $R_{\text{sp}}^{\text{total}}$, varying γ, and changing the scale in the axis to fit the measured plot below and above threshold. The crosses in Fig. 12(a) show our best fit to the experimental data that is

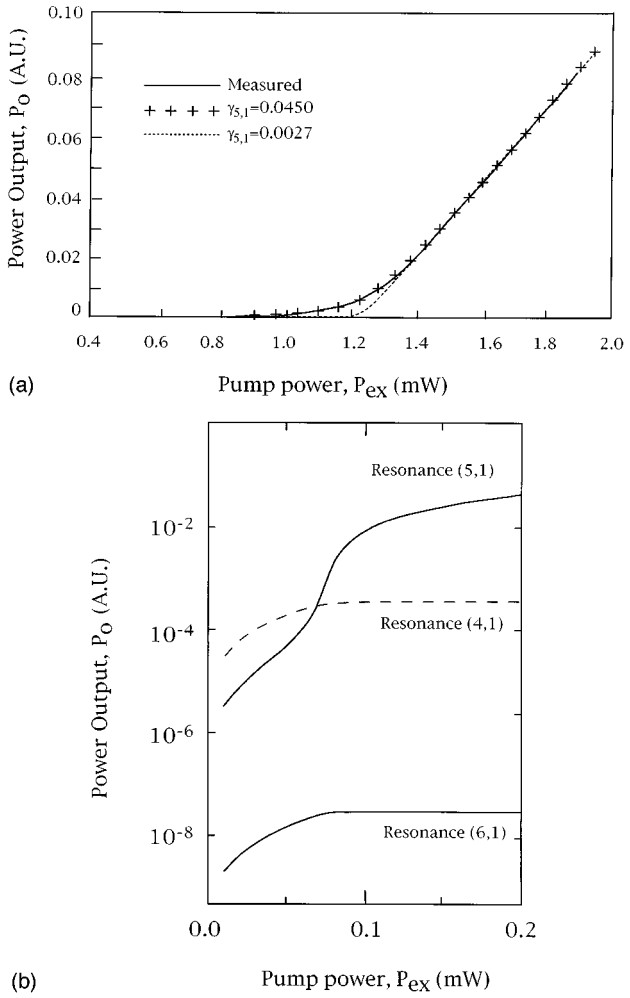

FIG. 12. (a) Measured scattered lasing power P_{out} to the top of the disk is plotted against the total insident pump power P_{ex} at the laser wavelength. The dotted line shows the calculated P_{out} vs P_{ex} plot after scaling for fitting the experimental result above and below threshold utilizing $\gamma_{5,1}=0.0027$ from the **k** broadening approach. The crosses show the best fit with $\gamma_{5,1}=0.045$. (b) Calculated P_{out} vs P_{ex} log plot for resonances (4,1), (5,1), and (6,1).

obtained when $\gamma_{5,1}=0.045$. This reasonably small value justifies our use of $N_{\text{BB}}(E)$, however, we note that for cavities with significantly higher coupling one should use the density of states $N(E)$ that includes free modes and all resonances.

It is somewhat difficult to establish a value for γ directly from a model of the microdisk cavity properties. Chu and Ho have shown that γ for cylindrical cross-section ring lasers is strongly influenced by geometrical properties.[19] We also expect γ for microdisk lasers to depend on resonant cavity properties. To study this problem, in principle one requires a complete, self-consistent description of all resonances. This includes the calculated two-dimensional resonances (quasi and nonquasiconfined states) and 3D confined and free-modes. This knowledge may then be applied to dynamic equations to obtain the relative intensity and linewidth of the resonances of interest and the spontaneous emission background. For a simple cavity geometry such as in a conventional edge-emitting laser, the modes are all described by resonances with two polarizations and propagation vector

$\mathbf{k}=(j\hat{\mathbf{x}}+k\hat{\mathbf{y}}+l\hat{\mathbf{z}})/V^{1/3}$ plus free modes, where V is the volume. Conventionally one assumes $V^{1/3}\gg\lambda$ and defines a continuous k space with a volume $V_k=8\pi^3/V$ per resonance. Neglecting free modes, a resonance density of $N(\hbar\omega)=8\pi n_{\text{eff}}^3\omega^2/hc^3$ is obtained and the contribution from spontaneous emission into a given Fabry–Perot mode ω_M^{FB} is $1/[N(\hbar\omega)V\Delta\omega_M^{\text{FB}}]$ where $\Delta\omega_M^{\text{FB}}$ is the separation between two adjacent Fabry–Perot modes.[20] Also, it is important to realize that typically the resonances in such a laser are lossy and, hence, the eigenvalues are complex with a frequency broadening $\Delta\omega\approx\omega/Q$. However, for large cavities defined by mirrors with reflectivity R such that $Q_{J,K,L}\leqslant -4\pi L/\lambda\ln(R)$, the resonance broadening is much narrower than the mode separation. In this situation the energy summation over modes to obtain $N(E)$ is justified. The question of how to deal with free modes is a more complicated issue since the k-space volume of a free mode depends on boundary conditions external to the cavity. One approach to resolve this issue is to assume a black-body distribution for the free modes of the laser that are in thermal equilibrium with their surroundings. If true, one then may evaluate the overlap integral between the calculated free-mode solid angle distribution and the lossy resonance $\mathbf{k}$ directions with associated broadening, $\Delta\mathbf{k}$. Here, we assume that the lossy eigenvector problem results in nonzero linewidth eigenvalues. In this case a broadening in $\mathbf{k}$ caused by the loss results in a broadening of the resonance spatial distribution. This spatial integral multiplied by the result obtained with energy summation represents the amount of spontaneous emission that could actually couple into resonant modes. For a large rectangular cavity this overlap will asymptotically approach unity and, hence, the free-mode correction becomes negligible.

The same approach may be applied to the microdisk laser. This requires a complete three-dimensional model for free modes and resonances for which part of the free-mode emission out of the disk's plane does not couple into resonances. Also, our solution for the two-dimensional problem involves resonances with higher, resonance-dependent, Q's (resonance broadening narrower than resonance intervals), plus the resonance distribution is not dense enough to allow a continuum approximation. This means that the number of modes in a given energy range cannot be obtained by an integral in k space nor can it be obtained by simply counting modes, since each mode is not equally broadened in frequency. As a first step we propose a normalized Lorentzian distribution for each mode

$$\Pi_{M,N}(\omega)=[\omega_{M,N}/\pi Q_{M,N}]/[(\omega-\omega_{M,N})^2+(\omega_{M,N}/Q_{M,N})^2], \tag{20}$$

that results in a mode count 1 when integrated over the entire spectrum. The total number of resonant modes in the frequency interval $\Delta\omega_{M,N}$ around resonance frequency $\omega_{M,N}$ is then

$$N(\hbar\omega)\Delta\omega=2\sum_{M,N}\int_{\omega_{M,N}-\Delta\omega_{M,N}/2}^{\omega_{M,N}+\Delta\omega_{M,N}/2}\prod_{M,N}(\omega)d\omega, \tag{21}$$

where the factor 2 accounts for the degeneracy $M=\pm|M|$. For the practical case we are considering, resonances (4,1), (5,1), and (6,1) all have high Q and linewidth narrower than their frequency separation, however, all the other resonances are wider and their contribution is approximately $(\Delta\omega_{M,N}Q_{M,N})/\pi\omega_{M,N}$. The free-modes in the plane, $M=0$, may be treated similarly, as they correspond to a continuum distribution in ω with a line broadening given by the black-body distribution for the system. This distribution is much wider than the spontaneous emission, and considering the normalization for mode counting in the frequency domain, it results in a very small contribution. Using this approach we obtain the fraction γ of total spontaneous emission that couples into resonances (4,1), (5,1), and (6,1) is $\gamma=0.122$, $\gamma=0.240$, and $\gamma=0.125$, respectively. These numbers are unpredictably large because we have not included 3D free modes. If we consider that only emission inside a cone with incidence angle smaller than the critical angle for a given n_{eff} will leave the disk, we obtain the maximum 3D free-mode spatial coupling of 0.93. This correction factor results in γ much higher than obtained by our fitting procedure and would lead to a thresholdless behavior for the laser. Alternatively, if one considers an angular broadening given by

$$\begin{aligned}\Delta tg\,\theta&\approx\Delta k_p/(n_{\text{eff}}\omega_{M,N}/c)\\&\approx(n/n_{\text{eff}})\Delta\omega_{M,N}/\omega_{M,N}\\&\approx(n/n_{\text{eff}})1/Q_{M,N},\end{aligned} \tag{22}$$

where k_p is the planar component of the lossy wave vector, we obtain what we believe is the minimal contribution from spontaneous emission $\gamma_{4,1}=0.0200$, $\gamma_{5,1}=0.0027$, and $\gamma_{5,1}=0.0002$. The dotted line in Fig. 12(a) shows the calculated P_{out} vs P_{ex} with these values of γ. In order to obtain a more accurate value for γ several other factors should be included in the calculation. For instance, photon recirculation and light piping through the pedestal are likely to occur. Photon recirculation results from high energy photons that get reabsorbed before leaving the disk. Because the path of in-plane confined emission is much longer than emission within the cone, recirculation is much more relevant for confined emission, thereby reducing the value of γ. Light piping occurs because the critical angle for the interface disk pedestal is much larger widening the off-plane emission. Again this should reduce γ. Besides geometrical arguments, carrier dynamics and fundamental spontaneous emission processes must be considered. In the first case, carrier diffusion may exist due to spatial separation of resonance and pumped active region given the nature of the WGM profile.[3] In the second case, a complete model of spontaneous emission should be able to accurately deal with the limit of $R\rightarrow 0$ in the presence of realistic boundary conditions. We are currently working towards a better understanding of these issues.

To calculate the spectrum we have used the lower bound value for γ, a pump wavelength of 0.85 μm with a 56% photon injection efficiency in the disk. Fig. 12(b) shows a log plot of P_{out} vs P_{ex} for resonances (4,1), (5,1), and (6,1). Below threshold resonance (4,1) has the highest power due to the greater contribution from spontaneous emission. At $P_{\text{ex}}=0.072$ mW resonance (5,1) starts lasing, clamping the carrier density at $n_{\text{th}}\approx 6.78\times 10^{18}$ cm^{-3}. A large discrepancy

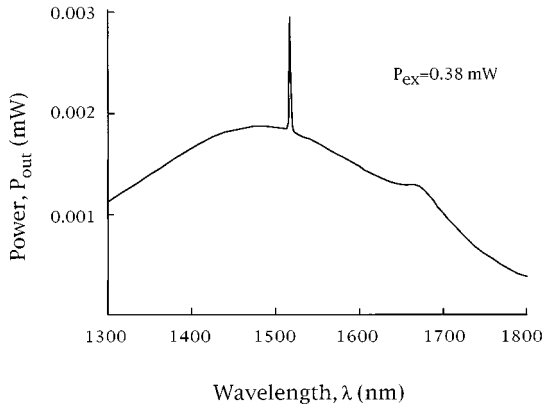

FIG. 13. Calculated spectrum at $P_{ex}=0.08$ mW. The absence of resonance (6,1), the relationship between resonance (4,1), (5,1), and the shape of the spectrum background show a great agreement with the experiment.

in threshold power as compared to the experimental result in Fig. 12(a) is a consequence of an overestimated pump efficiency and the absence of nonradiative processes and/or scattering losses in the model.

To calculate the spectrum we have assumed a Lorentzian line shape for the resonances

$$P(E,P_p)=\sum_{M=4}^{6}\frac{[\hbar\omega_{M,1}/2Q_{M,1}(P_p)]^2P_M(P_p)}{(E-\hbar\omega_{M,1})^2+[\hbar\omega_{M,1}/2Q_{M,1}(P_p)]^2}. \tag{23}$$

To this we add the calculated spontaneous emission power obtained at the clamped carrier density value. The spontaneous emission power output is given by $P_{sp}(\omega)=R_{sp}^{n=n_{eff}}(\omega)\times(V\Delta\omega)\hbar\omega$ where $\Delta\omega$ accounts for a 5 nm spectral resolution around ω. Figure 13 shows the calculated spectrum at $P_{ex}=0.08$ mW with the spontaneous emission reduced by a factor 4 to account for limitations in the detection optical system. The observed absence of mode (6,1), the relationship between resonance (4,1), (5,1), and the shape of the spectrum background show good agreement with the experimental data.

Our approach to modeling microdisk lasers includes the most important aspects of the physics determining device behavior. However, it is possible to construct improved but necessarily more complex models. An exact numerical calculation of the three-dimensional problem would allow a better estimate of the cavity Q. The antenna emission of such a system could give us a better description of the free-space distribution. Finally photon reabsorption and photon recirculation would have to be included to renormalize the spectral dependent carrier generation rate. Finally, we believe the narrowing of resonance (4,1) depends critically on the gain curve for energies between laser wavelength and band gap. In this region a better determination of the intraband relaxation time and its effect on renormalizing the electron band structure may be necessary to describe the available gain above threshold in this spectrally narrow transparent region.

SUMMARY

In summary, conformal mapping used to determine the radial and azimuthal eigenvalues and eigenvectors of leaky optical resonances present in dielectric microdisks appears to apply equally well to semiconductor microdisk lasers. A quantitative model to account for the presence of gain and loss in the microdisk describes reasonably well the dynamic dependence of output power and pump power, as well as the measured laser spectrum.

ACKNOWLEDGMENTS

This work is supported in part by the Joint Services Electronics Program under Contract No. F49620-94-0022 and the Advanced Research Projects Agency (ARPA) under contract No. MDA-972-94-1-0001.

APPENDIX

From Snyder and Love,

$$C(\xi)=\frac{|\mathrm{Ai}[\Delta\exp(2\pi i/3)]^{-2}}{4\pi|\Delta|^{1/2}}, \tag{A1}$$

where $\mathrm{Ai}(z)$ is the Airy function and

$$\Delta\equiv\{\cos^2\xi_c-\cos^2[\xi(M)]\}\times\{(\omega n_{\mathrm{eff}}^{\mathrm{TE(TM)}}/c)R/2\sin^2[\xi(M)]\}^{2/3}. \tag{A2}$$

For large M's, under the whispering gallery mode approximation $\xi(M)=(M-1)\pi/2M$, $\omega_{M,N}=x_M^N c/n_{\mathrm{eff}}R$. Δ reduces to

$$\Delta\rightarrow[\cos^2\xi_c](x_M^1/2)^{2/3}. \tag{A3}$$

The Airy function $\mathrm{Ai}(z)$ can be written in terms of modified Bessel functions such as $\mathrm{Ai}(z)=\pi^{-1}\sqrt{z/3}K_{1/3}(\frac{2}{3}z^{3/2})$,[21] that for large z has the asymptotic behavior $K_{1/3}(z)\rightarrow\sqrt{\pi/2z}\exp(-z)$.[22]

Since $\Delta\gg1$, then

$$C(\xi)\rightarrow\exp(-\tfrac{4}{3}\Delta^{3/2})=\exp[-\tfrac{2}{3}x_M^1\cos^2\xi_c], \tag{A4}$$

and for $\xi(M)\gg\xi_c$, $T(\xi)=C(\xi)$, we obtain

$$T_M=\exp[-(2\pi Rn_{\mathrm{eff}}/\lambda)(2/3)\cos^3\xi_c]. \tag{A5}$$

[1] S. L. McCall, A. F. J. Levi, R. E. Slusher, S. J. Pearton, and R. A. Logan, Appl. Phys. Lett. **60**, 289 (1992).
[2] A. F. J. Levi, R. E. Slusher, S. L. McCall, T. Tanbun-Ek, D. L. Coblentz, and S. J. Pearton, Electron. Lett. **28**, 1010 (1992).
[3] A. F. J. Levi, R. E. Slusher, S. L. McCall, S. J. Pearton, and W. S. Hobson, Appl. Phys. Lett. **62**, 2021 (1993).
[4] A. F. J. Levi, S. L. McCall, S. J. Pearton, and R. A. Logan, Electron. Lett. **29**, 1666 (1993).
[5] M. Hovinen, J. Ding, A. V. Nurmikko, D. C. Grillo, J. Han, L. He, and R. L. Gunshor, Appl. Phys. Lett. **63**, 3128 (1993).
[6] N. C. Frateschi and A. F. J. Levi, Appl. Phys. Lett. **66**, 2932 (1995).
[7] A. W. Snyder and J. D. Love, IEEE Trans. **MTT-23**, 134 (1975).
[8] N. C. Frateschi, A. P. Kanjamala, A. F. J. Levi, and T. Tanbun-Ek, Appl. Phys. Lett. **66**, 1859 (1995).
[9] M. Heiblum and J. H. Harris, IEEE J. Quantum Electron. **QE-11**, 75 (1975).
[10] M. K. Chin, D. Y. Chu, and S. T. Ho, J. Appl. Phys. **75**, 3302 (1994).
[11] S. W. Koch, F. Jahnke, and W. W. Chow, Semicond. Sci. Technol. **10**, 739 (1995). K. Henneburger, F. Herzel, S. W. Koch, R. Binder, A. E. Paul, and D. Scott, Phys. Rev. A **45**, 1853 (1992).

[12] S. L. Chuang, J. O'Gorman, and A. F. J. Levi, IEEE J. Quantum Electron. **QE-29**, 1631 (1993).
[13] E. O. Kane, J. Phys. Chem. Solids **1**, 249 (1957).
[14] H. Haug and S. Schmitt-Rink, Prog. Quantum Electron. **9**, 3 (1984).
[15] B. Sermage, D. S. Chemla, D. Sivco, and A. Y. Cho, IEEE J. Quantum Electron. **QE-22**, 774 (1986).
[16] See, G. D. Mahn, *Many Particle Physics* (Plenum, New York, 1986); D. Pines and P. Nozieres, *The Theory of Quantum Liquids* (Benjamin, New York, 1966).
[17] W. Bardyszewski and D. Yevick, Appl. Phys. Lett. **54**, 837 (1989).
[18] C. H. Henry, R. A. Logan, and K. A. Bertness, J. Appl. Phys. **52**, 4457 (1981).
[19] D. Y. Chu and S. T. Ho, J. Opt. Soc. Am. B **10**, 381 (1993).
[20] T.-P. Lee, C. A. Burrus, J. A. Copeland, A. G. Dentai, and D. Marcuse, IEEE J. Quantum Electron. **QE-18**, 1101 (1982).
[21] M. Abramowitz and I. A. Stegun, in *Handbook of Mathematical Functions* (Dover, New York, 1970), p. 447.
[22] G. Arfken, in *Mathematical Methods for Physicists* (Academic, New York, 1970), p. 517.